Accepted Manuscript

Title: Discrimination between abiotic and biotic drought stress in tomatoes using hyperspectral imaging

Authors: Nik Susič, Uroš Žibrat, Saša Širca, Polona Strajnar, Jaka Razinger, Matej Knapič, Andrej Vončina, Gregor Urek, Barbara Gerič Stare

Please cite this article as: Susič N, Žibrat U, Širca S, Strajnar P, Razinger J, Knapič M, Vončina A, Urek G, Stare BG, Discrimination between abiotic and biotic drought stress in tomatoes using hyperspectral imaging, *Sensors and Actuators: B. Chemical* (2018), https://doi.org/10.1016/j.snb.2018.06.121

Discrimination between abiotic and biotic drought stress in tomatoes using hyperspectral imaging

Nik Susič[1], Uroš Žibrat[1], Saša Širca[1], Polona Strajnar[1], Jaka Razinger[1], Matej Knapič[1], Andrej Vončina[1], Gregor Urek[1] and Barbara Gerič Stare[1]*

[1] Agricultural Institute of Slovenia, Plant Protection Department, Hacquetova ulica 17, 1000 Ljubljana, Slovenia

* Corresponding author: barbara.geric@kis.si, +386 1 2805 276

Highlights

- Detection and discrimination of plant stress origin using hyperspectral imaging.
- Nematode infestation can be reliably differentiated from the water deficiency.
- Abiotic drought resulted in the most obvious differences in the light spectrum.
- Identification of nematode infestation possible with specific spectral regions.
- Reliable prediction of nematode infestation even in early stages of infestation.

Abstract

Crop plants are subjected to various biotic and abiotic stresses. Both root-knot nematodes (biotic stress) and water deficiency (abiotic stress) lead to similar drought symptoms in the plant canopy. In this work, hyperspectral imaging was used for early detection of nematode infestation and water deficiency (drought) stress in tomato plants. Hyperspectral data in the range from 400 to 2500 nm of plants subjected to different watering regimes and nematode infestation levels were analysed by partial least squares - discriminant analysis (PLS-DA) and partial least squares - support vector machine (PLS-SVM) classification. PLS-SVM classification achieved up to 100 % accuracy differentiating between well-watered and water-deficient plants, and between 90 and 100 % when identifying nematode-infested plants. Grouping the data according to the time of imaging increased the accuracy of classification. Shortwave infrared spectral regions associated with the O-H and C-H stretches were most relevant for the identification of nematode infested plants and severity of infestation. This study demonstrates the capability of hyperspectral imaging to identify and discriminate between biotic and abiotic plant stresses.

1. **Introduction**

With the ever-increasing tendency for automation in agricultural practices [1] and the development of precision agriculture concepts [2,3], it is desirable to develop remote sensing technologies and applications. These include techniques for the assessment of soil properties, nutrient depletion, plant biomass, and weed detection. True to the idea of precision agriculture, this information can be used for site-specific management [4]. One of such technologies is the hyperspectral imaging, which was originally developed for Earth remote sensing applications [5]. In the context of geobotany, it had already been postulated that vegetation reflectance spectra in the $0.4 - 2.5$ μm region of light spectrum could contain information on plant pigment concentrations, leaf cellular structure and moisture content. Analysis of unique spectral signatures demonstrated the benefits of higher spectral resolution, having enabled discrimination of various plant species and communities. With regard to these results, Goetz et al. [5] opined that the analysis of various parts of reflectance spectra could be used in the detection of plant physiological condition and health, stress detection and characteristics, as well as assessment of the amount of biomass. Hyperspectral imaging devices record images consisting of numerous spatial image planes of the same object at different wavelengths. These spatial images are then superimposed one over another forming a three-dimensional data cube (hypercube) which is the hyperspectral image as recorded by the camera [6]. Hyperspectral images are thus composed of vector pixels, containing spectral information for a range of wavelengths in the electromagnetic spectra – typically used systems include the visible and near-infrared (VNIR: $400 - 1000$ nm) and shortwave infrared (SWIR: $1000 - 2500$ nm) regions [7]. Apart from geology-oriented applications, this technology has since inception been successfully used in many other areas such as microscopy [8], material classification [9], medical diagnostics [10], artwork and historical artefact analysis and conservation [11], and especially, food quality and safety assessment [12–15]. Analysing leaf reflectance at visible and infrared wavelengths can provide information about the plants, such as leaf pigmentation and physiological conditions [16], therefore, it is possible to utilise hyperspectral imaging for the early detection of plant diseases. Pathogens causing direct leaf damage can be detected with higher accuracy [17–21] but due to the ability of this technology to reveal hidden changes in plant physiology, it can be used to assess the often non-specific damage caused by root pathogens such as different plant-parasitic nematodes [22–24].

Root-knot nematodes (RKNs) from the genus *Meloidogyne* (Nematoda, Tylenchida, Meloidogynidae) are considered one of the most significant agricultural pests [25–27]. RKNs are plant endoparasites

that parasitize the root system. After entering the actively growing root, they elicit the development of a feeding site comprising several multinucleate "giant" cells, using oesophageal gland secretions. Through subsequent growth and development of nematodes, this feeding site gradually develops into a visible root gall. Development of root galls and further deformation of the root system leads to the overall weakening of the host plants due to reduced uptake of water and nutrients [28]. RKNs cause major economic damage and it has been estimated that losses on an annual basis amount to 5% of global agricultural production [29]. The worldwide economic damage caused by plant parasitic nematodes is estimated at around €110 billion per year [30]. RKN spread is becoming more pronounced as some populations of *Meloidogyne* spp. have genetically adapted to resistance factors commonly bred in economically important plant varieties, and many of older chemical nematicides like methyl bromide are not being registered for use because of health and environmental concerns [31,32]. This further emphasises the need to detect nematodes in the early stages of root infestation for effective management.

The most straightforward method to determine RKN infestation is visual examination of plant roots for the presence of root galls. However, this approach is invasive and impractical for large-scale use, additionally; the tell-tale galls gradually develop with time and vary in size depending on different RKN species and host plant. Application of remote sensing technologies such as hyperspectral imaging can in principle address these problems, however, plant reflectance is subjected to a complex plant tissue and canopy structure which makes such applications more difficult to develop and implement for large-scale use [4]. While RKNs cause specific galls on the roots of parasitized plants, the effect on the canopy is non-specific and similar to the signs of drought or nutrient depletion, and can be observed to the naked eye only in the last stages of nematode infestation. *Meloidogyne* spp. infestation of plants such as tomato (*Solanum lycopersicum*) can influence plant physiological parameters (e.g. photosynthesis) measured on the leaf canopy [33]. Strajnar et al. [34] have shown the potential of hyperspectral imaging to detect *Meloidogyne* spp. infestation. Further examples are detection of beet cyst nematode *Heterodera schachtii* and the fungal pathogen *Rhizoctonia solani* infesting sugar beet [22,23], detection of the sudden death syndrome and soybean cyst nematode (*Heterodera glycines*) in soybean [24] and examining the presence of plant-parasitic nematode *Rotylenchulus reniformis* in cotton fields [35]. Thus, it is possible to detect specific (biotic) stressors but difficulties can arise in the discrimination between different pathogens. Some stressors, e.g. water stress, are more accurately detected [36]. Furthermore, it can be difficult to integrate data from different sensors. Any remote sensing application to accurately detect RKN infestation in plants should reliably discriminate between abiotic drought stress symptoms and biotic stress caused by the

nematodes, the reason being a high similarity of above-ground effects caused by both stressors on the plant canopy.

The goals of this study were: 1) to evaluate the capability of VNIR and SWIR hyperspectral imaging of tomato leaf reflectance to detect symptoms caused by either abiotic stress due to drought, or biotic stress elicited by *M. incognita*; 2) to test supervised classification models to accurately differentiate between plants affected by abiotic or biotic stress as well as plants affected by both stressors; 3) to test supervised classification models to determine infestation intensity; 4) to describe the temporal variability of the hyperspectral imaging data in the experiment; and 5) to compare sensitivity of different approaches for biotic and abiotic stresses detection.

2. Materials and methods

2.1 Experimental design

The study was designed as a pot experiment in which a single plant per pot represented one biological replication. Plants (n = 42) were divided into 6 groups (treatments), each group contained 7 biological replicates (Table 1). The experiment was conducted in the controlled environment in the glasshouse at the Agricultural Institute of Slovenia (Ljubljana, Slovenia) from February to June 2016. Experiment was conducted using commercially available tomato (*S. lycopersicum*) hybrid 'Horus F1' (L'Ortolano, Italy) that had been ascertained to be susceptible to *M. incognita* infestation (data not shown). Tomato seeds were surface sterilised in 3% aqueous solution of sodium hypochlorite (NaOCl; Kemika, Croatia) prior to use and germinated *in vitro* on 1/3 Potato Dextrose Agar (PDA) medium (Biolife, Italy) for 6 days at T = 22°C in the dark. Sprouted seeds that did not show any bacterial or fungal contamination were transferred to sterile plant substrate and grown in trays in the glasshouse for 16 days. For planting a substrate mixture consisting of 2 parts fine-grain (MP1/G), 2 parts coarse-grain (MP4) quartz sand (Termit, Slovenia) and 1 part fine peat substrate Potgrond P (Klasmann-Deilmann, Germany) was used. The final bulk density of the substrate mixture was 1.25 g/cm^3. Afterwards, plantlets were transplanted into Styrofoam multitrays and grown for 35 days until the root system was well developed. Fifty-one-day old plants were finally transplanted to 25 cm-diameter polypropylene pots (V = 5 L) in the same substrate mixture and supported with 1.8 m high plastic-coated stakes. Temperature sensors iButton (Maxim, USA) were embedded into the substrate of three randomly spaced pots. Temperature data was used to follow the progression of *M. incognita* development and to predict the completion of the first reproduction cycle [37]. The average temperature as calculated from the measurements by substrate temperature sensors in the interval

from April 19th to May 23rd 2016 was 21.6°C. The first development cycle was predicted to be completed at 50 DAI, according to the model [37].

Individual plants were subjected to two different watering regimes to attain well-watered [W] conditions or to elicit the abiotic stress of chronic drought [D] (Table 1). Biotic stress was caused by RKN infestation. Plants received different levels of initial nematode inoculum at the time of final transplantation; no RKN [N], low inoculum [L] of $15×10^3$ *M. incognita* eggs per plant (equalling 3 eggs/cm^3 substrate) and high inoculum [H] of $250×10^3$ *M. incognita* eggs (equalling 50 eggs/cm^3 substrate). Plants were watered daily with a three-component nutrient mixture Flora Series (General Hydroponics Europe, France) for hydroponics-based systems. The nutrient mixture was prepared by mixing the Flora Series (N-P-K) solutions: FloraGro 3-1-7, FloraMicro 5-0-1 and FloraBloom 0-5-4, according to the manufacturer's guidelines with regard to the plant developmental stage. Water-deficient (drought) conditions were initiated 8 days after inoculation (DAI) of plants with the nematode eggs. Water-deficient plants were irrigated with the lowest volume of nutrient solution sustaining turgor pressure. Well-watered plants were irrigated to substrate saturation with the volume of nutrient solution providing adequate moisture until the nutrient solution started to leak out the bottom of the pots. Nutrient solutions were diluted in such a manner that all plants received the same amount of nutrients regardless of the watering regime. Due to deterioration that could not be attributed to either drought or nematode stress, data from one plant each from the DL, DH and WH treatment groups (Table 1) was excluded from the subsequent analyses.

2.2 Nematode inoculum preparation

The nematode *M. incognita* isolate from Nova Gorica, Slovenia was sustained in the glasshouse pot culture on *S. lycopersicum* cv. Val (Semenarna Ljubljana, Slovenia) tomato plants. Nematode-egg-suspension was prepared following the methodology by Hussey and Barker [38]. Infested roots were homogenised in 1% NaOCl for 3 min and washed with tap water through a stack of sieves with apertures of 850, 250, 63 and 32 μm (Retsch, Germany). Nematode eggs were collected from the last sieve, suspended in a defined volume and counted under a stereomicroscope Nikon SMZ800 (Nikon, Japan). The same method was used for final evaluation of nematode reproduction during the experiment. Total eggs were isolated from infested roots collected at the end of the experiment. Reproduction factor (Rf) was calculated as the total number of eggs isolated after experiment (P_f) divided by the initial number of eggs in the inoculum (P_i); ($Rf = P_f/P_i$).

2.3 Substrate moisture content

Substrate moisture content was determined gravimetrically. Substrate was sampled prior to hyperspectral imaging sessions at 12, 34, and 52 DAI in order to validate the difference between well-watered and water-deficient treatments. For gravimetric water content determination, substrate samples (~ 15 g) were taken from each pot at 5 cm depth and dried in the oven SP-105C (Kambič, Slovenia) for 24 hours at 105°C. Samples were weighed before and after drying and substrate moisture content (%) was calculated.

2.4 Photosynthesis parameters

General plant stress was assessed at 52 DAI. Gas exchange and chlorophyll *a* fluorescence measurements were taken on the youngest fully expanded leaf (usually the fifth leaf from the apical shoot) [39]. Gas exchange parameters (photosynthesis rate, transpiration rate and stomatal conductance) were measured in one sun-exposed leaf per plant with the LI-6400XT Portable Photosynthesis System (LI-COR Biosciences, Nebraska, USA) at ambient air temperature (20.2°C – 24.9°C), air humidity (Rh = 53.5% – 73.5%), reference CO_2 concentration (380 μmol mol^{-1}), and stable light intensity of 1000 μmol photons m^{-2} s^{-1} from an internal LED light source. Measurements were taken between 9:30 and 13:00. Chlorophyll *a* fluorescence parameters were measured with a Mini-PAM pulse-amplitude-modulated fluorometer (Heinz Walz GmbH, Germany). Maximum quantum efficiency of photosystem II (PSII) photochemistry (F_v/F_m) was measured on 10-min dark adapted leaves when all PSII reaction centers were open (State 1). It was calculated as $F_v/F_m = (F_m – F_0)/F_m$ by first measuring the minimal fluorescence (F_0) using a low intensity measuring light (0.15 μmol m^{-2}s^{-1} PAR), after which a saturating pulse (7000 μmol m^{-2}s^{-1} PAR for 0.8 s) was applied to close all PSII reaction centers (State 2) to measure maximal fluorescence (F_m). The parameters effective quantum yield of PSII (($F_{m'} - F_s)/F_{m'}$) and apparent electron transport rate (ETR = Yield × PPFD × 0.5 × 0.84) were measured on different, light adapted leaves, in order to avoid any influence of the light exposure history. $F_{m'}$ and F_s are the maximal fluorescence and steady-state fluorescence under light conditions, respectively; PPFD is the photosynthetic flux density incident on the leaf, 0.5 is the factor that assumes equal distribution of energy between the two photosystems, and 0.84 is the leaf absorbance factor [40,41]. Measurements were performed between 11:00 and 16:00. F_v/F_m was evaluated on one leaf per plant, whereas Yield and ETR were evaluated on five leaves per plant for all plants in the experiment.

2.5 Plant morphology

Plant morphology measurements (leaf area, plant height and plant dry weight) were taken at 52 DAI. Total leaf area was measured using LI-3100C Area Meter (LI-COR Biosciences). Plant height at the tip of apical shoot was measured before the plant material was cut into smaller pieces for dry weight measurement and dried in 2-litre paper bags at T = 55°C in the dryer VLE800 (Memmert, Germany) for 4 days.

2.6 Hyperspectral imaging

Hyperspectral imaging was conducted over time in the experimental glasshouse. The first imaging was conducted at 12 DAI, in the early stages of nematode infestation and initial plant response to different stressors (labelled S1); at 34 DAI, which corresponded to the middle of the nematode developmental cycle (labelled S2); and at 52 DAI, when nematodes were expected to complete the first reproduction cycle and produce egg-masses on the root surface (labelled S3). We used two pushbroom imaging spectrometers; HySpex VNIR (spectral range 400 – 988 nm) and SWIR (spectral range 950 – 2500 nm) (Norsk Elektro Optikk AS, Norway). The cameras were mounted horizontally on a tripod coupled with a rotation stage, so the rotation speed was synchronized with the scanning cameras frame rate and field of view. The system was controlled by the data acquisition unit using HySpex GROUND software as supplemented by the manufacturer. The imaging system setup included two calibrated halogen light sources with an even light intensity between 400 and 2500 nm and was positioned at 1.5 m from the ground level and 3 m distance from the imaged tomato plants – the resulting field of view per image was 1 × 2.5 m. Using this arrangement, up to 3 plants could be imaged at the same time against a black background screen. Every image also included a calibrated diffuse white reference plate with 95% reflectance (SphereOptics, Germany). Reflectance values for each band of every image pixel (R) were then calculated as:

$$R_i = \frac{I_i - D_i}{\frac{W_i - D_i}{0.95}}$$

, where I_i represents the reflected signal of the i-th band; W_i is the reflected t signal of the i-th band from the reference panel and D_i is the sensors' dark current of the i-th band [6].

2.7 Pre-processing and image analysis

Leaf-area pixels containing relevant spectral information had to be extracted from the images. The workflow (Fig. 1) was based on the guidelines described by Huang et al. [6] and Shrestha et al. [42].

Supervised classification using spectral information divergence [43] was performed on each image so leaf-area pixels could be extracted and used for further analysis. Pixel values of each plant were normalised using area normalization, due to the variable geometry of imaged plants, and mean spectra for each plant were calculated. Reflectance data were then smoothed by Savitzky-Golay filter using second-order polynomial, and second-order derivatives calculated to remove scattering effects in the spectra and emphasize small spectral variations not evident in the raw data. Prior to the development of classification models we used partial least squares - discriminant analysis (PLS-DA) [44] to explore the hyperspectral data for patterns among the tomato plants due to different stress treatments. Outliers were identified using Hotelling T^2 test. Variables were weighted using a standard deviation weighting process, and models were validated using full cross validation for PLS and 10-fold cross validation for partial least squares - support vector machine (PLS-SVM). Relevant spectral regions were evaluated by considering their correlations with PLS-DA factors. The PLS-DA factor scores were then used as input variables for support vector machine classification (PLS-SVM) [45,46]. The capacity factor (C) and gamma value for each PLS-SVM classification were determined by performing a grid search of several combinations of C and gamma on a log scale. The combinations giving the best accuracy were then used for model development and 10-fold cross-validation. Similar to PLS-DA, variables (PLS-factors) were weighted using standard deviation weighting. Analyses were first performed on pooled samples, from all three imaging sessions, and later separately for each imaging session. Finally, samples were analysed separately for well-watered and water-deficient plants, and infected plants alone, to determine the infection severity. Spectral signatures of each plant were separated and extracted using ENVI 5.1 (Harris Geospatial, USA). The extracted data were pre-processed, and PLS-SVM evaluation and VIP analyses performed in R [47], while PLS-DA and PLS-SVM classifications were performed in Unscrambler 10.3 (CAMO Software, Norway).

2.8 Statistical analysis

The data for parameters: total number of nematode eggs, Rf, leaf area, plant height, photosynthesis rate, transpiration rate, stomatal conductance, effective quantum yield of PSII, and F_v/F_m, were transformed using Box-Cox transformation to achieve normality. Data for plant dry weight and ETR were log-transformed due to the zero lambda value ($\lambda = 0$) obtained in the Box-Cox procedure. A two-way analysis of variance (ANOVA) was then used to test for the interaction of watering and nematode infestation effect on the measured parameters. Where statistically significant, the data were further analysed with Tukey's HSD (Honest Significant Difference) test at $\alpha = 0.05$ to separate means. Data for the total number of nematode eggs were analysed with Welch's ANOVA and Games-Howell post-hoc test because of unequal variances between groups for this parameter. Data were

presented as means with standard error of the mean ($\bar{n}$ ± SE) followed by statistical analyses results. Analyses were performed with R software suite [47]. Statistical evaluation of hyperspectral data was performed according to the workflow presented in Fig. 1.

3. Results

3.1 Nematode reproduction and plant morphology

Nematodes successfully multiplied in all inoculated plants (Table 2). There was a statistically significant interaction between the effects of watering and nematode infestation on plant morphology only for leaf area ($F_{2, 33}$ = 4.17, p = 0.024). Treatments primarily segregated into two groups according to the different watering regimes, so that water-deficient plants were typically lower in height, dry weight and leaf area. However, high density *M. incognita* infestation (treatments DH and WH) significantly affected plant dry weight (Table 2), while low density infestation (DL and WL) did not produce significant differences compared to non-infested plants (DN and WN).

3.2 Substrate moisture content

Substrate moisture content measurements showed a gradual development of chronic drought conditions in water-deficient treatments (data not shown). At 34 and 52 DAI, gravimetric water contents in well-watered treatments (WN, WL and WH) were on average three and two times greater, respectively, than in water-deficit treatments (DN, DL and DH). Gravimetric water content was not substantially different between well-watered and water-deficient treatment at 12 DAI.

3.3 Photosynthesis parameters

Assessments of photosynthesis (CO_2 exchange and chlorophyll *a* fluorescence) were used to confirm plant stress. The rate of photosynthesis, as well as stomatal conductance, transpiration and F_v/F_m differed significantly between treatments (Table 3). At the same time, the effective quantum yield of PSII and ETR were not significantly affected. Two-way ANOVA indicated that these parameters were significantly affected by the watering regime, while nematode infestation and interaction between the two were not significantly influenced. Stomatal conductance and transpiration differed significantly between well-watered (WN, WL and WH) and water-deficient plants (DN, DL and DH), but photosynthesis rate and F_v/F_m did not (Table 3).

3.4 Plant stress assessment using hyperspectral imaging

PLS-SVM classification of hyperspectral imaging data showed that it is possible to differentiate between biotic and abiotic drought stress in tomato plants (Fig. 2). However, separation between RKN infested and non-infested plants was less clear; treatment groups were not apparent. When differentiating between well-watered and water-deficient groups, PLS-SVM classification achieved an accuracy of 92 % Identification of infested plants achieved a success rate of 77 %, and was lowest at 24.6 % when identifying treatment groups. These results are showcased by PLS-SVM factor score plots (Fig. 2).

Because the variability of the data prevented the development of reliable models for treatment identification, we performed further analyses on data separated into three groups, according to the three imaging sessions (Fig. 2a). Imaging sessions were classified with a 95 % success rate using PLS-SVM. In pooled samples the main separation was along the first PLS-SVM factor, with reflectance at ranges 510-576, 606-693, 725-784, 905-909, 1047-1178, 1216-1265, 1330-1390, 1523-1553, 1830-1873, and 1906-2015 nm characterizing the differences (Fig. 3). Plants in drought stress showed lower reflectance in the green part of the visible spectrum and in NIR, and higher reflectance in the SWIR spectral region (Fig. 4a). When classifying imaging sessions the second PLS-SVM factor divided the third imaging session into two groups, according to water availability (Fig. 5a). The second factor was characterized by reflectance in the NIR and SWIR regions (increasing at ranges 930-959, 1402-1486, and 1876-1940 nm, and decreasing at ranges 950-1006, 1257-1324, 1600-1676, and 1705-1810 nm).

When data was separated into groups according to time of imaging, classification success of water stress in all three imaging groups (S1, S2, and S3) reached 100 % accuracy. The first factor again accounted for the main separation, in the NIR (increasing correlation at ranges 831-875 and 983-1009 nm, decreasing at 966-977 nm) and SWIR spectral regions (increasing correlation at 1254-1270 nm, and decreasing at 1140-1156 and 1390-1400 nm).

The separation between RKN infested and non-infested plants showed similar patterns in all three imaging sessions. The differences were characterized by reflectance at ranges 751-768, 842-857, 944-958, 1189-1216, 1270-1287, 1324-1346, 1493-1509, 1764-1786, and 1960-1977 nm. In the visible spectrum no apparent differences were observed, while infested plants showed a higher reflectance in NIR and lower in SWIR. PLS-SVM achieved a comparatively high success, with accuracy ranging from 90.5 % (S2) to 100 % (S1). When the data was further divided according to water availability,

identification success increased to 100 % for all imaging sessions, except for water-deficient plants in S3, where the accuracy was 95.2 %.

A similar trend in classification success was observed when identifying treatment groups of RKN infested plants. Pooled data of well-watered and water deficient plants yielded comparatively poor accuracies, with 50 % (S1) to 59.5 % (S3) correctly classified instances. Averaged spectra of all treatments showed a distinct division into two groups: (1) water deficient plants, and (2) well-watered plants (Fig. 4a). This division was further confirmed when the data was separated according to water availability. Classification success increased to a range of 78.6 % (S1) to 100 % (S3) in well-watered plants, and from 85.7 % (S1) to 100 % (S3) in water-deficient plants. Hence, reliability of the PLS-SVM classification increased in both water treatment groups, from S1 to S3 (Fig. 5, Table 4). In both water treatment groups, plants with lower initial inoculum showed higher reflectance in the SWIR region (ranges 1286-1313, 1482-1514, 1585-1612, 1775-1835, 1982-209, 2090-2112, and 2291-2308 nm), and lower at ranges 1395-1406, 1889-1917, and 2188-2221 nm. Furthermore, water-deficient plants exhibited another trend. From S1 to S3, spectral information also became relevant in the NIR (in S2; ranges 955-983, 1200-1222, 1548-1645, and 2091-2096 nm) and visible spectra (in S3; ranges 511-566, 704-737, 850-861, and 993-1015 nm).

4. Discussion

Our results demonstrate that it is possible to utilise hyperspectral imaging data combined with supervised learning classification to successfully discriminate between different types of stresses on tomato plants. In order to reliably differentiate between biotic stress from *M. incognita* and abiotic drought stress, it was necessary to elicit plant responses to both stressors separately and in combination in a controlled setting, since it is known that *M. incognita* infestation leads to general symptoms of water deficit stress [48]. Alterations in root anatomy (gall formation) lead to reduced water and nutrient uptake and retard plant growth and development. Effects can be quantified by measuring various physiological parameters like leaf water potential, root hydraulic conductivity, stomatal conductance [48,49] and net leaf photosynthesis [50,51], as well as various morphological characteristics of plants. We observed retarded plant growth as indicated by decreased leaf area, dry weight and plant height in water-deficient plants. Additionally, severely nematode-infested plants significantly differed in total dry weight (Table 2: DH, WH) indicating that severe RKN infestations can compound the effects on plant morphology produced by water deficit.

Although plant stress due to water deficit could be assessed with net leaf photosynthesis and chlorophyll *a* fluorescence, some of these parameters did not show statistically significant results at 52 DAI and, furthermore, did not allow discrimination between abiotic and biotic stresses (Table 3). The latter is in accordance with conclusion of Mahlein [52], who noted that chlorophyll fluorescence is sensitive to early stress reaction of a plant, but lacks the potential to identify a specific disease. Previous work by Strajnar et al. [33] on the other hand, showed that nematode-induced physiological stress in tomato can be determined by measuring root hydraulic conductivity, water potential, stomatal conductivity, transpiration and net photosynthesis. Strajnar et al. [33], however, measured net photosynthesis rate at 102 DAI which was a period nearly twice as long as in the present experiment. By that time the roots were infested by the second generation of nematodes and the damage to the root system was presumably much more severe. The effect of nematodes on the plant physiological parameters was therefore more likely to be observed than in our experiment.

In our experiment, water deficit led to expected effects in plants as measured by stomatal conductance and transpiration rates. Affected plants (DN, DL and DH) averaged 4-fold lower transpiration and 4 – 14-fold lower stomatal conductance as well-watered plants (Table 3; WN, WL and WH) which in turn affected photosynthesis. Stomatal conductance rate and transpiration are directly connected to photosynthesis [53,54] and lower levels suggest stomata closing and hence lower rates of CO_2 assimilation. Although the parameter Fv/Fm showed a statistically significant decrease at the highest inoculum level in well-watered plants (Table 3; WH), the same effect could not be observed in water-deficient plants (DH). A similar nematode inoculum-dependent F_v/F_m decrease has been observed by Schmitz et al. [55] studying sugar beet exposed to *Heterodera schachtii*. The study, however, did not examine the effect of abiotic drought on this parameter. Although we were able to assess general plant stress using gas exchange and chlorophyll *a* measurements, these methods were not as sensitive as hyperspectral imaging. This may be attributed to the way in which the measurements are obtained using different systems – gas exchange and chlorophyll *a* is measured at a single point per plant, while hyperspectral imaging records the signal across the whole plant canopy. Local physiological abnormalities could affect a point measurement much more than the hyperspectral imaging measurement of a larger area.

Leaf senescence changes reflectance characteristics, the spectra of a proceeding senescence form an ordinal order [56]. These changes are mainly linked to the degradation of pigments (e.g. chlorophylls) and reallocation of resources. Plants in drought stress reallocate these resources to leaves with a higher potential. This is showcased by the identified relevant spectral ranges in our study. In the visible part of the spectrum only two ranges were identified, green and red, indicating changes in

pigment structure. The other spectral ranges (in NIR and SWIR) are linked to physical and chemical characteristics, such as cellulose and lignin [57], as well as carbohydrates, proteins, and water content [58]. Wavelengths in the ranges 966-977, 983-1009, 1216-1265, 1254-1270, and 1330-1390 nm are linked to the O-H stretch in water, while the range 1047-1178 nm is linked to the N-H stretch of proteins [59]. The prevalence of pigment and water content related wavelengths indicates the importance of these variables for classification of plants into age groups and drought stress.

Some of the identified spectral bands are known to be related to certain physiological variables, which indicate drought stress, in many plant species [60]. The lower reflectance around 535 nm is linked to an increase in zeaxanthin content, leading to the photoprotective state of the zeaxanthin cycle [61], while the decrease at 550 nm is related to adjustments of anthocyanins and other photoprotective pigments [62]. On the other hand, an increase of reflectance at 1500 nm is linked to a decrease of leaf water content [63]. Peñuelas et al. [64] showed that the water absorption band at 950-970 nm can be used to estimate water deficiency in plants. Our results corroborate the findings of Peñuelas et al. [64] only in part, as this spectral range was identified to be relevant only when data was separated according to imaging session, but not in pooled samples.

As plants matured and RKN infestations became more established, the relevant spectral ranges began shifting toward the visible spectrum (from S1 to S3). In S3, plants subjected to biotic and abiotic stress at the same time showed visible signs of stress, mostly in the green part of the spectrum (511-566 nm). The damage due to both abiotic and biotic stress became severe enough for the symptoms to become visible, and overshadow the foliar water content (at 1390-1520 nm, and 1860-2080 nm). Furthermore, for the identification of infested plants and severity of infestation, the O-H stretch became less important, and was replaced by the C-H stretch of carbohydrates and proteins (1189-1222 and 1324-1346 nm). This indicates the importance of wavelengths linked to pigments, and leaf chemistry and structure for identification of RKN infestations and their intensity.

Hyperspectral imaging enabled reliable identification of the water status of tomato plants in the experiment, as well as determination whether these plants were parasitized by nematodes (Fig. 5, Table 4). Water-deficient and well-watered plants could be predicted most reliably (classification success from 92 % to 100 %, depending whether data is pooled from imaging sessions) indicating that water-deficiency produced most readily observable changes in the spectrum of reflected light. It has been demonstrated that stress conditions influence production and / or transport of various substances throughout the plant tissues [51]. Drought induces metabolic changes in the plant through increased accumulation of free sugars and free essential amino acids that are involved in the

maintenance of host-plant osmotic balance. Drought can also lead to the increased production of defence compounds like protease inhibitors and the oxidative enzymes [51]. The hyperspectral camera system used in this study records light in the spectral range 409 – 2509 nm in 3.7 – 5.5 nm wide spectral channels, and could thus obtain detailed reflectance information and record spectral changes following the accumulation, transport flux or degradation of various chemicals, such as those that are induced by drought conditions. Various pigments like chlorophylls and carotenoids are normally examined since the concentration of these pigments is usually indicative of a physiological status of plants [5]. Pigment concentration in combination with spatial distribution mapping is particularly successful approach for prediction of various plant diseases that affect the leaves directly [20,65]. Nematode infestation could be predicted more reliably within the group of well-watered plants (WN, WL ,WH; classification success 100 %) than within the water-deficient plants (DN, DL, DH; classification success 95%) indicating that the specific spectral fingerprints determining nematode attack are being masked by drought-induced effects. Specific spectral indices that can classify soil-borne pathogen infestations including phytopathogenic fungi and plant-parasitic nematodes have been determined previously [35,22–24]. Even though identification of drought stress and its source, biotic or abiotic, was successful in our study, further research will be necessary to determine which physiological and structural changes in leaves account for the observed spectral differences between infested and non-infested plants. Accumulation, reduction or specific spatial distribution patterns of different compounds could not only determine the ability for hyperspectral imaging to detect different plant diseases and pests, but also serve as the basis for determination of disease/pest-specific spectral fingerprints. Nematode-stress specific spectral fingerprints could then be used to develop robust disease/pest and stress discrimination models that would be appropriated in remote sensing applications in various environments, such as the laboratory, greenhouse or in the field [66].

5. Conclusions

The study showed hyperspectral imaging can discriminate between abiotic and biotic stresses in tomato plants. High reliability discrimination was possible in the early stages of symptom manifestation and improved over time. Measurements of photosynthetic rate and chlorophyll *a* fluorescence at the completion of the first reproduction cycle showed that these parameters can be used to distinguish between well-watered and water-deficient plants, but not between nematode-infested and non-infested plants. The same trend was observed after examination of morphology such as plant dry weight, height and total leaf area. Statistically significant differences were observed between non-infested and highly infested plants for leaf area and plant dry weight, but not for the plants with lower nematode-infestation levels. Using PLS-DA and PLS-SVM classification on the

hyperspectral data, it was possible to discriminate between water-deficient and well-watered plants, and to determine nematode parasitized plants in both groups: water-deficient plants and well-watered plants. This demonstrates the capability of hyperspectral imaging for the identification and discrimination of biotic and abiotic plant stresses. To our knowledge, this study represents the first application of hyperspectral imaging to accurately discriminate between drought-induced abiotic and nematode-elicited biotic stresses in tomato plants.

This data could be further implemented for the development of remote sensing applications to detect nematode infestations in the field which would enable quicker response and more targeted pest management (e.g. the targeted use of chemical and / or biological control agents). Technology could be further implemented for breeding purposes for nematode resistance evaluation testing. As the climate changes and resulting higher average temperatures lead to more severe droughts and facilitate the development and spread of soil-borne pests like the tropical plant-parasitic nematodes of the genus *Meloidogyne*. Remote sensing applications in agriculture could be used to address these challenges in modern crop production. Some RKN species are emerging pests which are capable of producing several generations per season under favourable environmental conditions. Their population dynamics and reproduction time are mainly temperature dependent. Currently, they present a problem predominantly in greenhouses, where temperatures are higher and more stable than in the fields. Our field observations and population models in conjunction with climate change models indicate that RKNs will be able to produce more than two generations per season in the open fields. The introduction of RKN pest species into non-infested field or area can happen by different pathways (e.g infested plant material, infested agricultural machinery etc.) and it is usually introduced at one or several spots/ points. The initial distribution of the pest in the growing area is therefore in patches. At these introduction points the initial pest population develops over time and the spots gradually develop into bigger infested patches and may spread even further by human assistance (eg. with agricultural machinery). Infestation of the whole field or area is only expected few years after initial introduction of the pest when RKN population density increases with time. Any introduction of novel pest is easier to manage when it is not yet widely distributed. It is therefore very important to detect the pest before it has been spread onto the large area and with the use of hyperspectral imaging it is possible to detect infestation in its early stages, when only small and/or few patches of the growing area are infested. Current detection methods are destructive, each plant has to be uprooted and checked visually for presence of galls on the roots. While this approach is accurate, it is time consuming and not applicable in large areas when the extent of infestation has to be defined on the field. On the contrary, localization and estimation of nematode infestation extent in the field would be feasible, efficient and much faster using hyperspectral remote sensing

approach. A non-invasive early detection method would therefore have direct applications in agriculture.

The novel finding presented in this work is that with the use of hyperspectral imaging detection of root-knot nematode (*Meloidogyne* spp.) infestation of the plant is possible. Further, nematode infestation can be reliably differentiated from the water deficiency (abiotic stress) which causes similar symptom on the above ground parts of the plants. There is no other reliable method to predict nematode infestation without physical examination of plant roots, which is a disruptive method as the plant needs to be removed from the soil. Additional novelty in this work is information that shortwave infrared spectral regions associated with the O-H and C-H stretches were most relevant for the identification of nematode infested plants and severity of infestation. This indicates the importance of wavelengths linked to pigments, and leaf chemistry and structure for identification of RKN infestations and their intensity.

Conflict of Interest: The authors declare no conflict of interest.

References

[1] N. Wang, N. Zhang, M. Wang, Wireless sensors in agriculture and food industry - Recent development and future perspective, Comput. Electron. Agric. 50 (2006) 1–14. doi:10.1016/j.compag.2005.09.003.

[2] H. Melakeberhan, Embracing the emerging precision agriculture technologies for site-specific management of yield-limiting factors, J. Nematol. 34 (2002) 185–188.

[3] N. Zhang, M. Wang, N. Wang, Precision agriculture—a worldwide overview, Comput. Electron. Agric. 36 (2002) 113–132. doi:10.1016/S0168-1699(02)00096-0.

[4] W.S. Lee, V. Alchanatis, C. Yang, M. Hirafuji, D. Moshou, C. Li, Sensing technologies for precision specialty crop production, Comput. Electron. Agric. 74 (2010) 2–33. doi:10.1016/j.compag.2010.08.005.

[5] A.F.H. Goetz, G. Vane, J.E. Solomon, B.N. Rock, Imaging spectrometry for earth remote sensing, Science. 228 (1985) 1147–1153. doi:10.1126/science.228.4704.1147.

[6] H. Huang, L. Liu, M. Ngadi, Recent developments in hyperspectral imaging for assessment of food quality and safety, Sensors. 14 (2014) 7248–7276. doi:10.3390/s140407248.

[7] S. Sankaran, A. Mishra, R. Ehsani, C. Davis, A review of advanced techniques for detecting plant diseases, Comput. Electron. Agric. 72 (2010) 1–13. doi:10.1016/j.compag.2010.02.007.

[8] R.A. Schultz, T. Nielsen, J.R. Zavaleta, R. Ruch, R. Wyatt, H.R. Garner, Hyperspectral imaging: A novel approach for microscopic analysis, Cytometry. 43 (2001) 239–247. doi:10.1002/1097-0320(20010401)43:4<239::AID-CYTO1056>3.0.CO;2-Z.

[9] P. Tatzer, M. Wolf, T. Panner, Industrial application for inline material sorting using hyperspectral imaging in the NIR range, Real-Time Imaging. 11 (2005) 99–107. doi:10.1016/j.rti.2005.04.003.

[10] G. Lu, B. Fei, Medical hyperspectral imaging: a review, J. Biomed. Opt. 19 (2014) 010901–010901. doi:10.1117/1.JBO.19.1.010901.

[11] C. Fischer, I. Kakoulli, Multispectral and hyperspectral imaging technologies in conservation: current research and potential applications, Stud. Conserv. 51 (2006) 3–16.

[12] M.S. Kim, Y.R. Chen, P.M. Mehl, others, Hyperspectral reflectance and fluorescence imaging system for food quality and safety, Trans. ASAE. 44 (2001) 721–730.

[13] D. Lorente, N. Aleixos, J. Gómez-Sanchis, S. Cubero, O.L. García-Navarrete, J. Blasco, Recent advances and applications of hyperspectral imaging for fruit and vegetable quality assessment, Food Bioprocess Technol. 5 (2012) 1121–1142. doi:10.1007/s11947-011-0725-1.

[14] L.M. Dale, A. Thewis, C. Boudry, I. Rotar, P. Dardenne, V. Baeten, J.A.F. Pierna, Hyperspectral imaging applications in agriculture and agro-food product quality and safety control: A review, Appl. Spectrosc. Rev. 48 (2013) 142–159. doi:10.1080/05704928.2012.705800.

[15] D. Wu, D.-W. Sun, Advanced applications of hyperspectral imaging technology for food quality and safety analysis and assessment: A review — Part I: Fundamentals, Innov. Food Sci. Emerg. Technol. 19 (2013) 1–14. doi:10.1016/j.ifset.2013.04.014.

[16] W. Huang, D.W. Lamb, Z. Niu, Y. Zhang, L. Liu, J. Wang, Identification of yellow rust in wheat using in-situ spectral reflectance measurements and airborne hyperspectral imaging, Precision Agric. 8 (2007) 187–197. doi:10.1007/s11119-007-9038-9.

[17] M. Zhang, Z. Qin, X. Liu, S.L. Ustin, Detection of stress in tomatoes induced by late blight disease in California, USA, using hyperspectral remote sensing, Int. J. Appl. Earth. Obs. Geoinf. 4 (2003) 295–310. doi:10.1016/S0303-2434(03)00008-4.

[18] T. Rumpf, A.-K. Mahlein, U. Steiner, E.-C. Oerke, H.-W. Dehne, L. Plümer, Early detection and classification of plant diseases with Support Vector Machines based on hyperspectral reflectance, Comput. Electron. Agric. 74 (2010) 91–99. doi:10.1016/j.compag.2010.06.009.

[19] A.-K. Mahlein, U. Steiner, C. Hillnhütter, H.-W. Dehne, E.-C. Oerke, Hyperspectral imaging for small-scale analysis of symptoms caused by different sugar beet diseases, Plant Methods. 8 (2012) 3. doi:10.1186/1746-4811-8-3.

[20] A.-K. Mahlein, T. Rumpf, P. Welke, H.-W. Dehne, L. Plümer, U. Steiner, E.-C. Oerke, Development of spectral indices for detecting and identifying plant diseases, Remote Sens. Environ. 128 (2013) 21–30. doi:10.1016/j.rse.2012.09.019.

[21] W. Kong, F. Liu, C. Zhang, Y. Bao, J. Yu, Y. He, Fast detection of peroxidase (POD) activity in tomato leaves which infected with *Botrytis cinerea* using hyperspectral imaging, Spectrochim. Acta A Mol. Biomol. Spectrosc. 118 (2014) 498–502. doi:10.1016/j.saa.2013.09.009.

[22] C. Hillnhütter, A.-K. Mahlein, R.A. Sikora, E.-C. Oerke, Remote sensing to detect plant stress induced by *Heterodera schachtii* and *Rhizoctonia solani* in sugar beet fields, Field Crops Res. 122 (2011) 70–77. doi:10.1016/j.fcr.2011.02.007.

[23] C. Hillnhütter, A.-K. Mahlein, R.A. Sikora, E.-C. Oerke, Use of imaging spectroscopy to discriminate symptoms caused by *Heterodera schachtii* and *Rhizoctonia solani* on sugar beet, Precision Agric. 13 (2012) 17–32. doi:10.1007/s11119-011-9237-2.

[24] S.G. Bajwa, J.C. Rupe, J. Mason, Soybean Disease Monitoring with Leaf Reflectance, Remote Sens. 9 (2017) 127. doi:10.3390/rs9020127.

[25] J.N. Sasser, Worldwide dissemination and importance of the root-knot nematodes, *Meloidogyne* spp., J. Nematol. 9 (1977) 26–29.

[26] D.L. Trudgill, V.C. Blok, Apomictic, polyphagous root-knot nematodes: exceptionally successful and damaging biotrophic root pathogens, Annu. Rev. Phytopathol. 39 (2001) 53–77. doi:10.1146/annurev.phyto.39.1.53.

[27] D.P. Bebber, T. Holmes, S.J. Gurr, The global spread of crop pests and pathogens: The global spread of crop pests and pathogens, Glob. Ecol. Biogeogr. 23 (2014) 1398–1407. doi:10.1111/geb.12214.

[28] P. Abad, B. Favery, M.-N. Rosso, P. Castagnone-Sereno, Root-knot nematode parasitism and host response: molecular basis of a sophisticated interaction, Mol. Plant Pathol. 4 (2003) 217–224. doi:10.1046/j.1364-3703.2003.00170.x.

[29] J.N. Sasser, C .C. Carter, Overview of the international Meloidogyne project 1975-1984, in: C.C. Carter, J.N. Sasser (Eds.), An Advanced treatise on *Meloidogyne*, Volume I: Biology and Control, Department of Plant Pathology of the North Carolina State University and the United States Agency for International Development, Raleigh, 1985, pp. 19–24.

[30] E.G.J. Danchin, M.-J. Arguel, A. Campan-Fournier, L. Perfus-Barbeoch, M. Magliano, M.-N. Rosso, M. Da Rocha, C. Da Silva, N. Nottet, K. Labadie, J. Guy, F. Artiguenave, P. Abad, Identification of novel target genes for safer and more specific control of root-knot nematodes from a pan-genome mining, PLoS Pathog. 9 (2013) e1003745. doi:10.1371/journal.ppat.1003745.

[31] V.L. Fuller, C.J. Lilley, P.E. Urwin, Nematode resistance, New Phytol. 180 (2008) 27–44. doi:10.1111/j.1469-8137.2008.02508.x.

[32] W. Wesemael, M. Moens, N. Viaene, Root-knot nematodes (*Meloidogyne* spp.) in Europe, Nematology. 13 (2011) 3–16. doi:10.1163/138855410X526831.

[33] P. Strajnar, S. Širca, G. Urek, H. Šircelj, P. Železnik, D. Vodnik, Effect of *Meloidogyne ethiopica* parasitism on water management and physiological stress in tomato, Eur. J. Plant Pathol. 132 (2012) 49–57. doi:10.1007/s10658-011-9847-6.

[34] P. Strajnar, U. Žibrat, M. Knapič, S. Širca, B. Gerič Stare, G. Urek, Hyperspectral remote sensing as a new approach for early root-knot nematode detection, in: S. Širca, B. Gerič Stare, J. Razinger (Eds.), Plant Health for Sustainable Agriculture: Book of Abstracts, Agricultural Institute of Slovenia, Ljubljana, 2015, p. 120.

[35] R.A. Doshi, R.L. King, G.W. Lawrence, Classification of *Rotylenchulus reniformis* numbers in cotton using remotely sensed hyperspectral data on self-organizing maps, J. Nematol. 42 (2010) 179–193.

[36] T.A. Wheeler, H.W. Kaufman, Relationship of aerial broad band reflectance to *Meloidogyne incognita* density in cotton, J. Nematol. 35 (2003) 48–57.

[37] S. Širca, P. Strajnar, M. Knapič, U. Žibrat, G. Urek, Modelling of temperature dependent development of tropical root-knot nematode species, in: Proceedings of the 6th International Congress of Nematology, Cape Town, 2014, p. 142. http://nematologia.com.br/wp-content/uploads/2014/05/6thproc.pdf (accessed November 8, 2017).

[38] R.S. Hussey, K.R. Barker, Comparison of methods of collecting inocula for *Meloidogyne* spp., including a new technique, Plant Dis. Reptr. 57 (1973) 1025–1028.

[39] S. Haupt-Herting, K. Klug, H.P. Fock, A new approach to measure gross CO_2 fluxes in leaves. Gross CO_2 assimilation, photorespiration, and mitochondrial respiration in the light in tomato under drought stress, Plant Physiol. 126 (2001) 388–396.

[40] H.K. Lichtenthaler, C. Buschmann, M. Knapp, How to correctly determine the different chlorophyll fluorescence parameters and the chlorophyll fluorescence decrease ratio RFd of leaves with the PAM fluorometer, Photosynthetica. 43 (2005) 379–393. doi:10.1007/s11099-005-0062-6.

[41] M.D. Brooks, K.K. Niyogi, Use of a pulse-amplitude modulated chlorophyll fluorometer to study the efficiency of photosynthesis in *Arabidopsis* plants, in: Chloroplast research in *Arabidopsis*, Humana Press, Totowa, NJ, 2011: pp. 299–310. doi:10.1007/978-1-61779-237-3_16.

[42] S. Shrestha, M. Knapič, U. Žibrat, L.C. Deleuran, R. Gislum, Single seed near-infrared hyperspectral imaging in determining tomato (*Solanum lycopersicum* L.) seed quality in association with multivariate data analysis, Sens. Actuators B Chem. 237 (2016) 1027–1034. doi:10.1016/j.snb.2016.08.170.

[43] Y. Du, C.-I. Chang, H. Ren, C.-C. Chang, J.O. Jensen, F.M. D'Amico, New hyperspectral discrimination measure for spectral characterization, Opt. Eng. 43 (2004) 1777–1786.

[44] D. Ballabio, V. Consonni, Classification tools in chemistry. Part 1: linear models. PLS-DA, Anal. Methods. 5 (2013) 3790. doi:10.1039/c3ay40582f.

[45] A.I. Belousov, S.A. Verzakov, J. von Frese, Applicational aspects of support vector machines, J. Chemom. 16 (2002) 482–489. doi:10.1002/cem.744.

[46] J. Lv, L. Dai, Application of partial least squares support vector machines (PLS-SVM) in spectroscopy quantitative analysis, in: 6th World Congress on Intelligent Control and Automation, Institute of Electrical and Electronics Engineers Inc., Dalian, 2006, pp. 5228–5232. doi:10.1109/WCICA.2006.1713389.

[47] R Core Team, R: A language and environment for statistical computing, R Foundation for Statistical Computing, Vienna, Austria, 2015. https://www.R-project.org/.

[48] T.L. Kirkpatrick, D.M. Oosterhuis, S.D. Wullschleger, Interaction of *Meloidogyne incognita* and water stress in two cotton cultivars, J. Nematol. 23 (1991) 462–467.

[49] T.L. Kirkpatrick, M.W. Van Iersel, D.M. Oosterhuis, Influence of *Meloidogyne incognita* on the water relations of cotton grown in microplots, J. Nematol. 27 (1995) 465–471.

[50] D. Schwarz, H.-P. Kläring, M.W. Van Iersel, K.T. Ingram, Growth and photosynthetic response of tomato to nutrient solution concentration at two light levels, J. Am. Soc. Hortic. Sci. 127 (2002) 984–990.

[51] M.G. Ximénez-Embún, F. Ortego, P. Castañera, Drought-stressed tomato plants trigger bottom-up effects on the invasive *Tetranychus evansi*, PLoS One. 11 (2016) e0145275. doi:10.1371/journal.pone.0145275.

[52] A.-K. Mahlein, Plant disease detection by imaging sensors – parallels and specific demands for precision agriculture and plant phenotyping, Plant Dis. 100 (2016) 241–251. doi:10.1094/PDIS-03-15-0340-FE.

[53] M.M. Chaves, J. Flexas, C. Pinheiro, Photosynthesis under drought and salt stress: regulation mechanisms from whole plant to cell, Ann. Bot. 103 (2009) 551–560. doi:10.1093/aob/mcn125.

[54] J. Flexas, J. Bota, J. Galmés, H. Medrano, M. Ribas-Carbó, Keeping a positive carbon balance under adverse conditions: responses of photosynthesis and respiration to water stress, Physiol. Plant. 127 (2006) 343–352. doi:10.1111/j.1399-3054.2006.00621.x.

[55] A. Schmitz, I.I. Tartachnyk, S. Kiewnick, R.A. Sikora, W. Kühbauch, Detection of *Heterodera schachtii* infestation in sugar beet by means of laser-induced and pulse amplitude modulated chlorophyll fluorescence, Nematology. 8 (2006) 273–286. doi:10.1163/156854106777998755.

[56] M.N. Merzlyak, A.A. Gitelson, O.B. Chivkunova, V.Y. Rakitin, Non-destructive optical detection of pigment changes during leaf senescence and fruit ripening, Physiol. Plant. 106 (1999) 135–141. doi:10.1034/j.1399-3054.1999.106119.x.

[57] X. Li, C. Sun, B. Zhou, Y. He, Determination of hemicellulose, cellulose and lignin in Moso bamboo by near infrared spectroscopy, Sci. Rep. 5 (2015) srep17210. doi:10.1038/srep17210.

[58] J. Qiao, M.O. Ngadi, N. Wang, C. Gariépy, S.O. Prasher, Pork quality and marbling level assessment using a hyperspectral imaging system, J. Food Eng. 83 (2007) 10–16. doi:10.1016/j.jfoodeng.2007.02.038.

[59] W. Yin, C. Zhang, H. Zhu, Y. Zhao, Y. He, Application of near-infrared hyperspectral imaging to discriminate different geographical origins of Chinese wolfberries, PLoS One. 12 (2017) e0180534. doi:10.1371/journal.pone.0180534.

[60] P.J. Zarco-Tejada, V. González-Dugo, L.E. Williams, L. Suárez, J.A.J. Berni, D. Goldhamer, E. Fereres, A PRI-based water stress index combining structural and chlorophyll effects: Assessment using diurnal narrow-band airborne imagery and the CWSI thermal index, Remote Sens. Environ. 138 (2013) 38–50. doi:10.1016/j.rse.2013.07.024.

[61] J. Gamon, J. Penuelas, C. Field, A narrow-waveband spectral index that tracks diurnal changes in photosynthetic efficiency, Remote Sens. Environ. 41 (1992) 35–44. doi:10.1016/0034-4257(92)90059-S.

[62] M.R. Steele, A.A. Gitelson, D.C. Rundquist, M.N. Merzlyak, Nondestructive estimation of anthocyanin content in grapevine leaves, Am. J. Enol. Vitic. 60 (2009) 87–92.

[63] J.U.H. Eitel, P.E. Gessler, A.M.S. Smith, R. Robberecht, Suitability of existing and novel spectral indices to remotely detect water stress in *Populus* spp., For. Ecol. Manage. 229 (2006) 170–182. doi:10.1016/j.foreco.2006.03.027.

[64] J. Peñuelas, J. Piñol, R. Ogaya, I. Filella, Estimation of plant water concentration by the reflectance Water Index WI (R900/R970), Int. J. Remote Sens. 18 (1997) 2869–2875. doi:10.1080/014311697217396.

[65] Y.-R. Zhao, X. Li, K.-Q. Yu, F. Cheng, Y. He, Hyperspectral imaging for determining pigment contents in cucumber leaves in response to angular leaf spot disease, Sci. Rep. 6 (2016). doi:10.1038/srep27790.

[66] M. Govender, P.J. Dye, I.M. Weiersbye, E.T.F. Witkowski, F. Ahmed, Review of commonly used remote sensing and ground-based technologies to measure plant water stress, Water SA. 35 (2009) 741–752.

Author Biographies

Nik Susič received his MSc in biotechnology from the University of Ljubljana, Slovenia in 2014. He is currently working as a PhD student at the Department for Plant Protection of the Agricultural Institute of Slovenia, Slovenia. His research interests are hyperspectral detection of biotic and abiotic plant stress, plant-parasitic nematodes (*Meloidogyne* spp.) and novel strategies for soil-borne pest management.

Dr Uroš Žibrat is a researcher at the Plant Protection Department of the Agricultural Institute of Slovenia, with a background in environmental studies and freshwater ecology. His research focuses on imaging spectroscopy of plant pathogens and diseases, early detection of diseases and stress states, and pest and disease modelling.

Dr Saša Širca established himself as a researcher in the field of phyto-nematology after obtaining his PhD in 2007. His current research is covering the diagnostics of plant parasitic nematodes, biodiversity and epidemiology, integrated pest management, and environmentally friendly technologies for plant protection. He has participated in and managed several national and international research projects.

Dr Polona Strajnar received her PhD 2012, having researched in depth a species of root-knot nematode *Meloidogyne luci*. She continues to work at the Agricultural Institute of Slovenia in the field of plant-parasitic nematodes. Her research and expertise covers identification of nematodes, interactions of plants-plant parasitic nematodes, biotic plant protection, entomopathogenic nematodes, and plant physiology.

Dr Jaka Razinger completed his PhD in 2008. He is currently employed as a researcher at the Agricultural Institute of Slovenia, conducting research related to biotic pest control, integrated pest management, agricultural entomology, entomopathogenic fungi, applied microbiology, as well as analyses of plant physiology related to various stressors.

MSc**. Matej Knapič** is currently a researcher at the Agricultural Institute of Slovenia. He started his professional career as soil scientist and has been working as a GIS and remote sensing expert in plant health for the last 10 years. His research interest includes the hyperspectral imaging in the field of plant health and broader.

Dr Andrej Vončina is currently positioned as a researcher at the Plant Protection Department of the Agricultural Institute of Slovenia working in the field of integrated pest management. He is specialised in plant physiology analyses, having experience in measuring physiological responses of plants to various stress factors since the completion of his PhD in 2015.

Dr Gregor Urek is leading the Plant Protection Department at the Agricultural Institute of Slovenia. He completed his PhD in 1987 and has more than 30 years of work experience in the field of plant protection. His work encompasses the coordination of the expert work performed by the department for the Administration of the Republic of Slovenia for Food Safety, Veterinary Sector and Plant Protection, as well as being directly involved in research activities of the department. He is further involved in various expert commissions nationally and internationally.

Dr Barbara Gerič Stare completed her PhD in 2004. Since 2005, she is working as a researcher at the Plant Protection Department of Agricultural Institute of Slovenia in the field of plant parasitic nematodes and other plant pathogens. Her major research focus is in molecular identification, molecular phylogeny, variability and molecular evolution of parasitic factors (effectors) of plant-parasitic nematodes, plant-pathogen (virus, bacteria) and plant-pest (plant-parasitic nematodes) interactions, as well as in the implementation of quality management systems. She has also been involved in several national and international research projects.

Figure legends:

Fig. 1. Hyperspectral data analysis workflow based on Huang et al. [6] and Shrestha et al. [42].
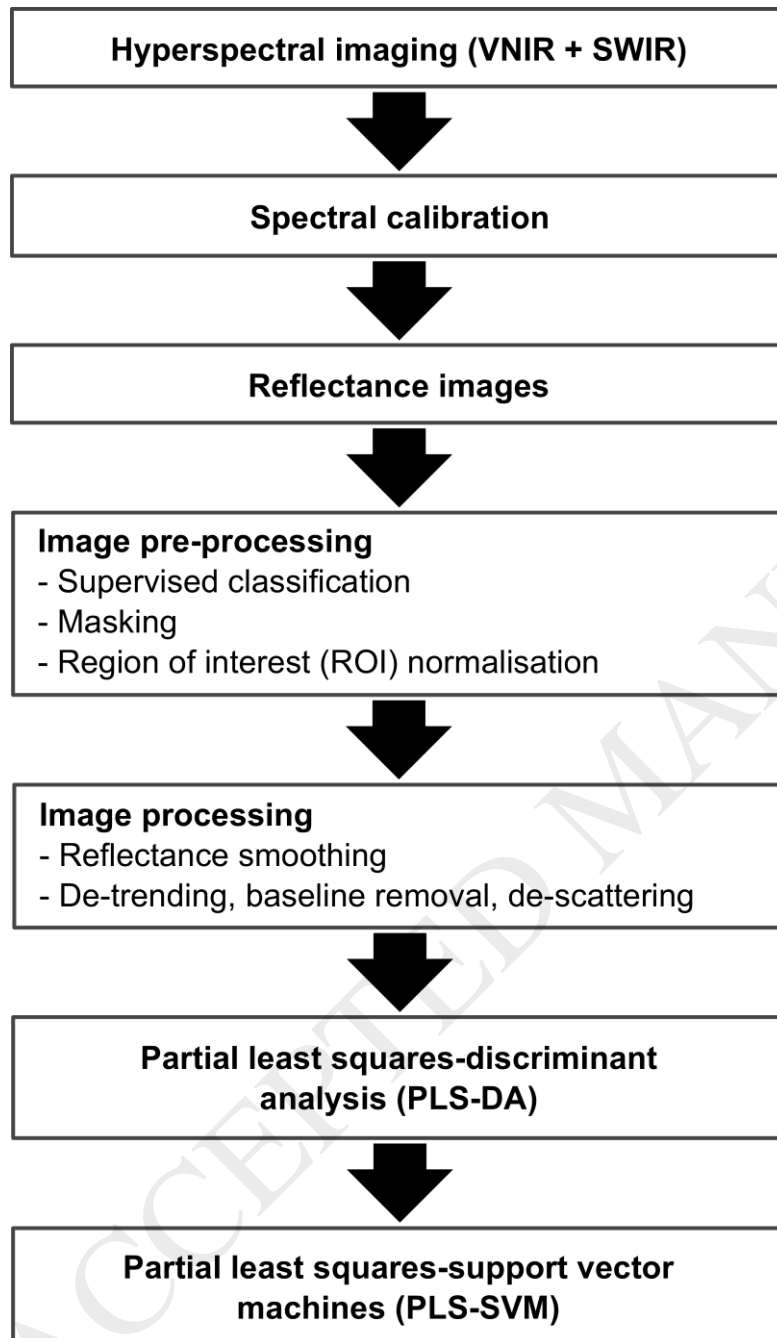

Fig. 2. PLS-SVM score plots showing variation in the plant groups with regard to: a) imaging session, b) water availability, c) RKN infestation, and d) treatment. In d) the abbreviations 'D' and 'W' denote drought and watered treatment, respectively and correspond to treatments defined in Table 1. Below the figures are the confusion matrices for each classification, denoted by the same letters as their corresponding figure (a, b, c, and d).
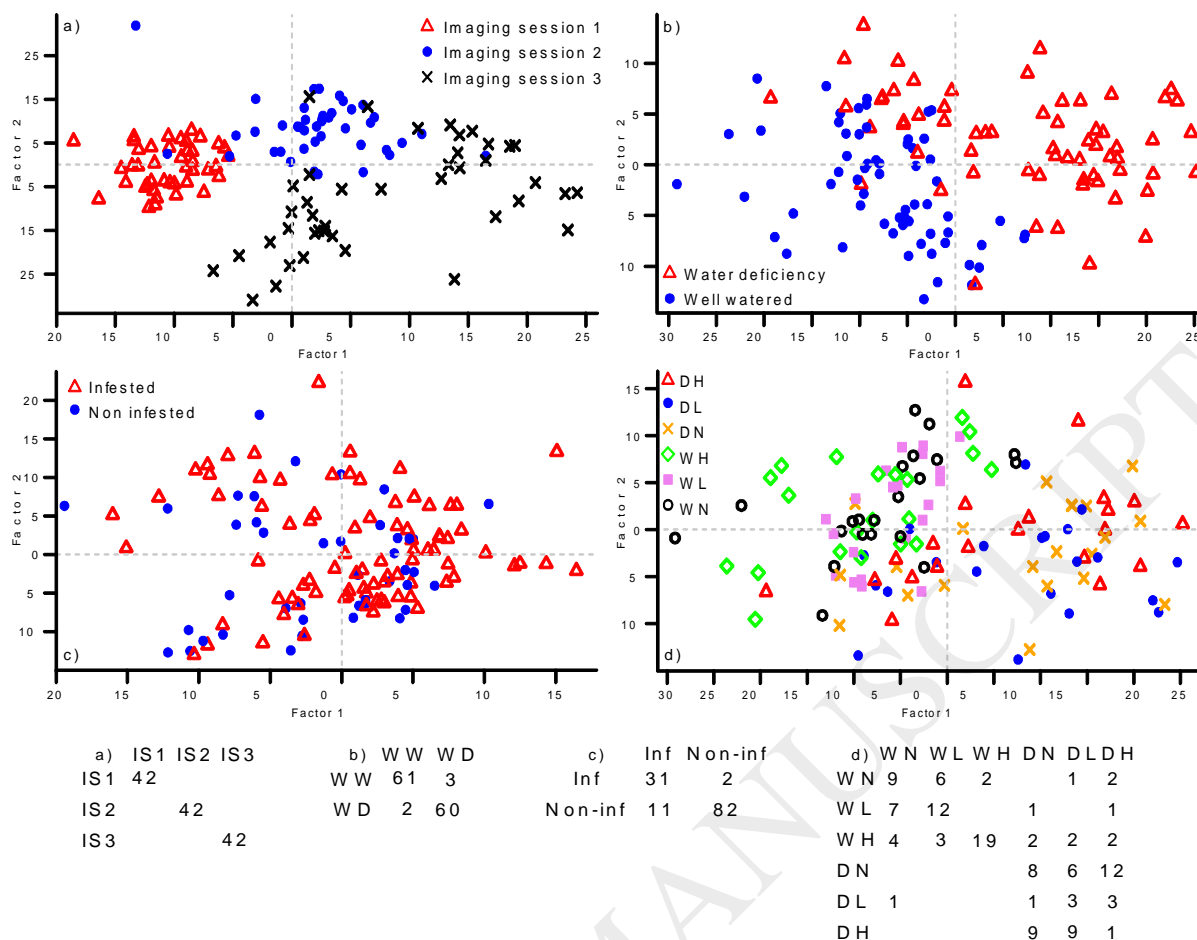
Fig. 3. Loadings of the first PLS-DA component for pooled samples. The black lines mark spectral ranges with correlations above 0.7 or below -0.7.
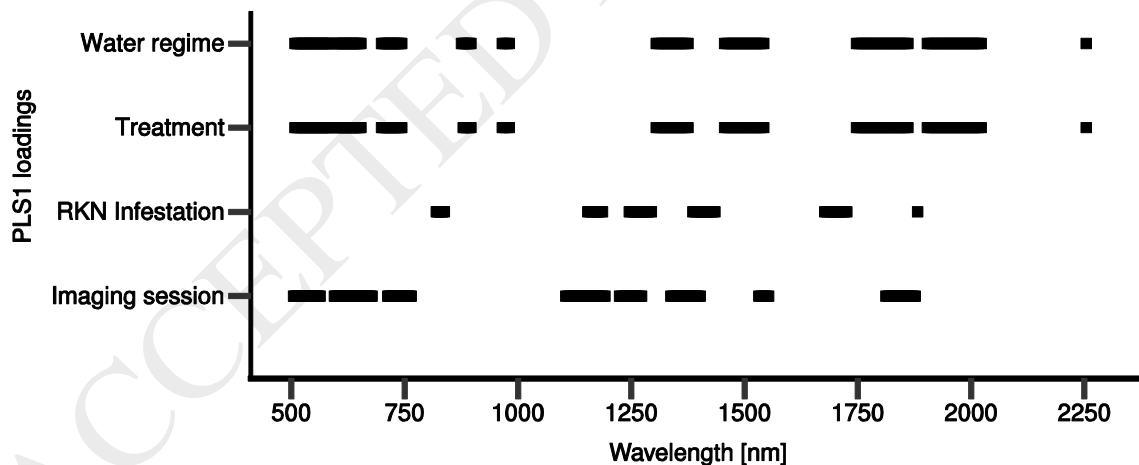

Fig. 4. Average normalized spectral signatures of plants grouped according to: a) water availability; b) imaging session (S1-3); and c) RKN infestation. Because of the area normalization process the y-axis is not in reflectance units.
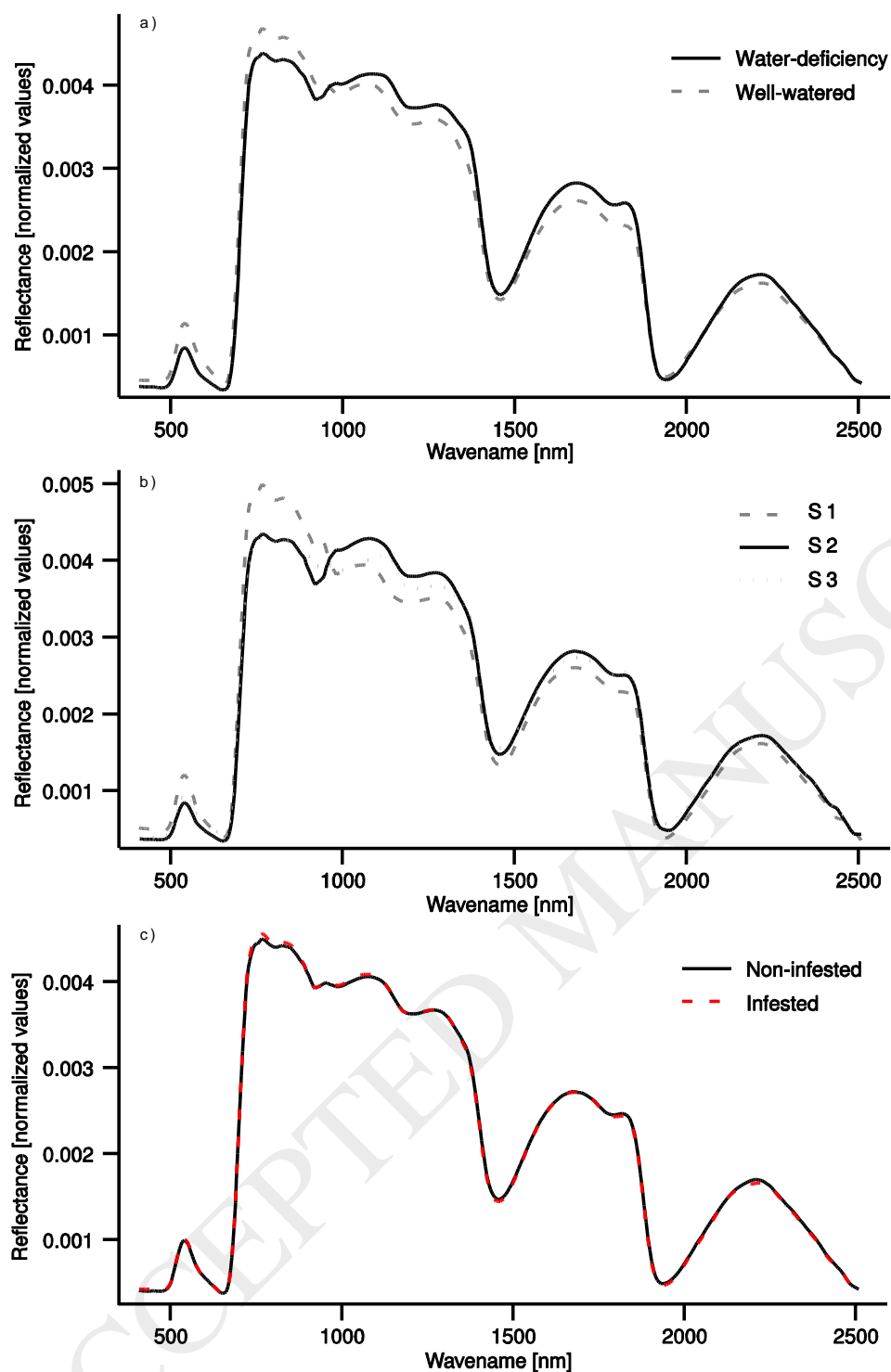
Fig. 5. PLS-SVM score plots showing the variation between treatment groups in imaging session 3 (S3). a) pooled data; b) watered plants; and c) water-deficient plants. Confusion matrices of each classification are inset in the figures. Classification of pooled data achieved a 59 % success rate, while both separated groups attained 100 % accuracy.
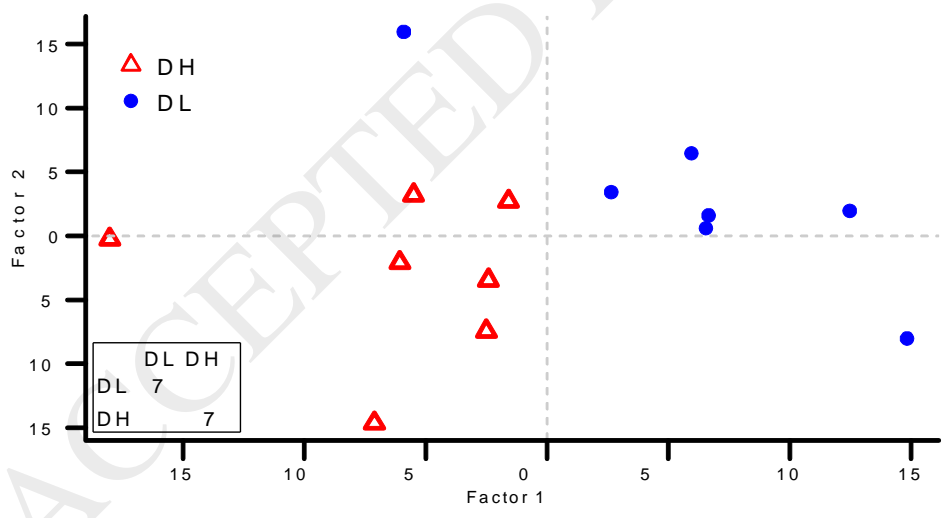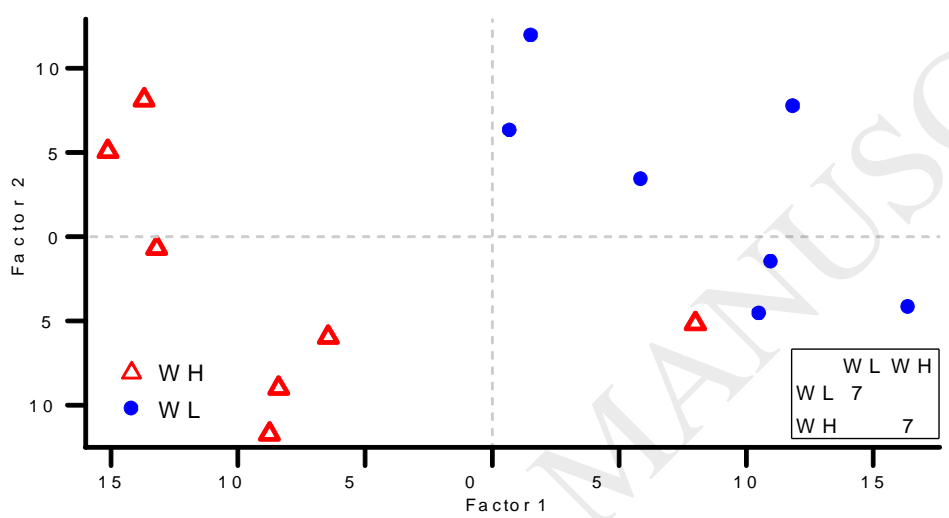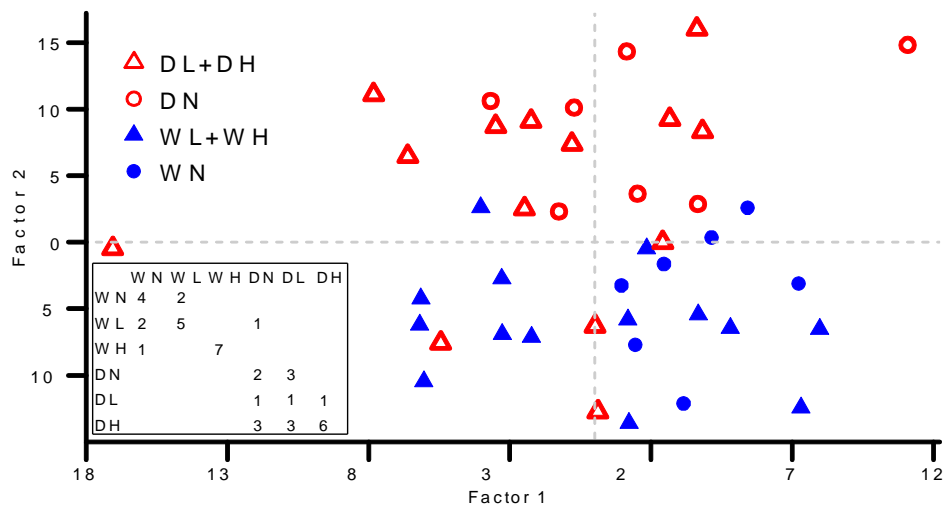
Table legends:

Table 1 Tomato plants were subjected to two watering regimes (well-watered [W] / water-deficient / drought [D]) and different levels of initial nematode inoculum (no RKN [N] / low inoculum [L] of 15×10^3 *Meloidogyne incognita* eggs per plant / high inoculum [H] of 250×10^3 *M. incognita* eggs per plant).

Table 2 Nematode reproduction and plant morphology parameters at 52 DAI in different treatments. Data expressed as treatment means with standard error (± SE), ANOVA statistics and Tukey's HSD test results. Means that share a letter are not significantly different at $p < 0.05$.

Table 3 Physiological parameters assessing plant photosynthesis and chlorophyll a fluorescence at 52 DAI in different treatments. Data expressed as treatment means ± SE, two-way ANOVA statistics and Tukey's HSD test results. Means that share the same letter are not significantly different at $p < 0.05$.

Table 4 Summary of PLS-DA and PLS-SVM analyses. The abbreviations used in the table are: Var – explained variance of the selected PLS components; RMSECV – root mean squared error of cross-validation of selected PLS components; c – SVM cost of classification parameter; gamma – SVM Gaussian kernel parameter; Ts – train set; CV – cross-validation.

Table 1 Tomato plants were subjected to two watering regimes (well-watered [W] / water-deficient / drought [D]) and different levels of initial nematode inoculum (no RKN [N] / low inoculum [L] of 15×10^3 *Meloidogyne incognita* eggs per plant / high inoculum [H] of 250×10^3 *M. incognita* eggs per plant).

Treatment abbreviation	Watering regime	RKN Infestation
WN		None
WL	Well-watered	Low inoculum
WH		High inoculum
DN		None
DL	Water-deficient (drought)	Low inoculum
DH		High inoculum

Table 2 Nematode reproduction and plant morphology parameters at 52 DAI in different treatments. Data expressed as treatment means with standard error (± SE), ANOVA statistics and Tukey's HSD test results. Means that share a letter are not significantly different at p < 0.05.

Treatment	Nematode eggs ($\bar{n} \times 10^6$)	Reproduction factor (Rf)	Leaf area (cm^2)	Plant height (cm)	Plant dry weight (g)
WN	0.0 ± 0.0 n/a	0.0 ± 0.0 n/a	3133.5 ± 75.9 a	158.1 ± 3.3 a	64.9 ± 0.7 a
WL	0.9 ± 0.2 b	56.6 ± 15.2	3103.4 ± 169.9 a	160.7 ± 2.7 a	61.4 ± 1.3 a
WH	8.6 ± 1.5 a	34.5 ± 5.8	2421.4 ± 86.0 b	150.5 ± 5.7 a	43.7 ± 3.9 b
DN	0.0 ± 0.0 n/a	0.0 ± 0.0 n/a	2360.6 ± 53.1 b	111.1 ± 3.6 b	25.8 ± 0.3 c
DL	0.8 ± 0.1 b	55.2 ± 9.1	2059.3 ± 126.1 b	116.7 ± 2.0 b	23.8 ± 0.3 c
DH	12.1 ± 0.9 a	48.5 ± 3.4	2035.5 ± 58.5 b	104.2 ± 2.2 b	17.3 ± 0.4 d
ANOVA statistics					
Watering		$F_{1, 23} = 1.10$, p = 0.306	$F_{1, 33} = 76.05$, **p < 0.0001**	$F_{1, 33} = 267.61$, **p < 0.0001**	$F_{1, 33} = 719.89$, **p < 0.0001**
Nematode	$^{(i)}F_{3, 10.04} = 58.54$, **p < 0.0001**	$F_{1, 23} = 1.21$, p = 0.284	$F_{2, 33} = 12.47$, **p < 0.0001**	$F_{2, 33} = 5.43$, **p = 0.009**	$F_{2, 33} = 52.07$, **p < 0.0001**
Interaction		$F_{1, 21} = 0.69$, p = 0.414	$F_{2, 33} = 4.17$, **p = 0.024**	$F_{2, 33} = 0.18$, p = 0.829	$F_{2, 33} = 0.13$, p = 0.879

$^{(i)}$ Welch's ANOVA does not test for the interaction effects of independent variables.

n/a – not applicable

Table 3 Physiological parameters assessing plant photosynthesis and chlorophyll a fluorescence at 52 DAI in different treatments. Data expressed as treatment means ± SE, two-way ANOVA statistics and Tukey's HSD test results. Means that share the same letter are not significantly different at p < 0.05.

Treatment	Photosynthesis rate (µmol CO_2 m-2 s-1)	Stomatal conductance (mol H_2O m^{-2} s^{-1})	Transpiration (mmol H_2O m^{-2} s^{-1})	Effective quantum yield of PSII	ETR (µmol e- m^{-2}s^{-1})	Fv/Fm
WN	5.57 ± 0.40 ab	0.09 ± 0.01 a	1.39 ± 0.10 a	0.71 ± 0.02	19.46 ± 1.42	0.77 ± 0.01 ab
WL	6.62 ± 0.84 a	0.12 ± 0.02 a	1.85 ± 0.31 a	0.71 ± 0.01	21.28 ± 2.28	0.77 ± 0.01 ab
WH	6.04 ± 1.07 ab	0.14 ± 0.04 a	1.99 ± 0.46 a	0.66 ± 0.03	17.53 ± 2.12	0.74 ± 0.01 b
DN	2.90 ± 0.64 bc	0.03 ± 0.00 b	0.37 ± 0.05 b	0.68 ± 0.02	20.99 ± 2.52	0.79 ± 0.01 a
DL	1.65 ± 0.72 c	0.02 ± 0.01 b	0.32 ± 0.08 b	0.69 ± 0.02	15.70 ± 1.42	0.79 ± 0.01 a
DH	3.59 ± 0.91 abc	0.03 ± 0.01 b	0.55 ± 0.08 b	0.67 ± 0.02	15.97 ± 0.93	0.79 ± 0.01 a
ANOVA statistics						
Watering	$F_{1, 33}$ = 28.34, **p < 0.0001**	$F_{1, 33}$ = 66.86, **p < 0.0001**	$F_{1, 33}$ = 67.46, **p < 0.0001**	$F_{1, 33}$ = 0.55, p = 0.462	$F_{1, 33}$ = 1.37, p = 0.251	$F_{1, 33}$ = 20.81, **p < 0.0001**
Nematode	$F_{2, 33}$ = 0.39, p = 0.682	$F_{2, 33}$ = 1.28, p = 0.292	$F_{2, 33}$ = 1.09, p = 0.348	$F_{2, 33}$ = 1.90, p = 0.166	$F_{2, 33}$ = 1.52, p = 0.235	$F_{2, 33}$ = 1.69, p = 0.200
Interaction	$F_{2, 33}$ = 1.62, p = 0.213	$F_{2, 33}$ = 1.07, p = 0.354	$F_{2, 33}$ = 1.18, p = 0.320	$F_{2, 33}$ = 0.61, p = 0.551	$F_{2, 33}$ = 1.40, p = 0.261	$F_{2, 33}$ = 1.39, p = 0.263

Table 4 Summary of PLS-DA and PLS-SVM analyses. The abbreviations used in the table are: Var – explained variance of the selected PLS components; RMSECV – root mean squared error of cross-validation of selected PLS components; c – SVM cost of classification parameter; gamma – SVM Gaussian kernel parameter; Ts – train set; CV – cross-validation.

Analysis		Imaging session [S]	Treatments	PLS-DA		SVM		Accuracy [%]	
				Var [%]	RMSECV	c	gamma	Ts	CV
Water deficiency-pooled		S1-3	all treatments	75	0.25	1	0.1	96	92.1
Infestation-pooled		S1-3	all treatments	37	0.45	1	0.1	89.7	77
Treatment-pooled		S1-3	all treatments	20.4	0.38	1	0.143	41.3	24.6
Imaging session		S1-3	all treatments	81	0.17	1	0.1	100	94.4
Water deficiency		S1	DN, DL, DH	95.8	0.11	100	0.01	100	100
Water deficiency		S2	DN, DL, DH	98.3	0.07	100	0.01	100	100
Water deficiency		S3	DN, DL, DH	98.5	0.07	100	0.01	100	100
Infestation	pooled	S1	DL, DH, WL, WH	93	0.11	10	0.01	100	100
	water deficiency	S1	DL, DH	98	0.06	0.01	0.01	100	100
	well-watered	S1	WL, WH	98	0.05	10	0.01	100	100
Infestation	pooled	S2	DL, DH, WL, WH	81	0.2	4.64	0.032	100	90.5
	water deficiency	S2	DL, DH	97	0.08	10	0.01	100	100
	well-watered	S2	WL, WH	99	0.05	100	0.01	100	100
Infestation	pooled	S3	DL, DH, WL, WH	79	0.21	0.52	0.01	100	92.9
	water deficiency	S3	DL, DH	94	0.12	46.4	0.001	100	95.2
	well-watered	S3	WL, WH	97	0.07	100	0.01	100	100
Treatment	pooled	S1	all treatments at S1	52	0.46	13.3	0.01	100	50
	water deficiency	S1	DL, DH	99	0.07	21.5	0.01	100	85.7
	well-watered	S1	WL, WH	99	0.08	10	0.01	100	78.6
Treatment	pooled	S2	all treatments at S2	55.8	0.49	3.59	0.1	69.05	54.8
	water deficiency	S2	DL, DH	99	0.02	10	0.01	100	92.9
	well-watered	S2	WL, WH	99	0.02	10	0.1	100	92.9
Treatment	pooled	S3	all treatments at S3	54	0.26	35.9	0.028	97.6	59.5
	water deficiency	S3	DL, DH	99	0.02	10	0.01	100	100
	well-watered	S3	WL, WH	99	0.01	35.9	0.01	100	100